



Deposited via The University of Leeds.

White Rose Research Online URL for this paper:

<https://eprints.whiterose.ac.uk/id/eprint/156214/>

Version: Accepted Version

Article:

Yazdi, R, Ghasemi, HM, Abedini, M et al. (2019) Oxygen Diffusion Layer on Ti–6Al–4V Alloy: Scratch and Dry Wear Resistance. *Tribology Letters*, 67 (4). 101. ISSN: 1023-8883

<https://doi.org/10.1007/s11249-019-1214-3>

© 2019, Springer Nature. This is an author produced version of an article published in *Tribology Letters*. Uploaded in accordance with the publisher's self-archiving policy.

Reuse

Items deposited in White Rose Research Online are protected by copyright, with all rights reserved unless indicated otherwise. They may be downloaded and/or printed for private study, or other acts as permitted by national copyright laws. The publisher or other rights holders may allow further reproduction and re-use of the full text version. This is indicated by the licence information on the White Rose Research Online record for the item.

Takedown

If you consider content in White Rose Research Online to be in breach of UK law, please notify us by emailing eprints@whiterose.ac.uk including the URL of the record and the reason for the withdrawal request.

Oxygen diffusion layer on Ti–6Al–4V alloy: scratch and wear resistance

R. Yazdi^a, H.M. Ghasemi^{a*}, M. Abedini^b, C. Wang^c, A. Neville^c

a: School of Metallurgy and Materials Engineering, College of Engineering, University of Tehran, Tehran, Iran

b: Department of Metallurgy and Materials Engineering, Faculty of Engineering, University of Kashan, Kashan, Iran

c: Institute of Functional Surfaces, School of Mechanical Engineering, University of Leeds, Leeds, LS2 9JT, UK

*Corresponding author. Tel: +98 2161114095, E-mail address: hghasemi@ut.ac.ir (H.M. Ghasemi).

Abstract

Oxygen diffusion layer (ODL) was produced on Ti–6Al–4V by thermal oxidation at a temperature of 850 °C for 3 and 6 h. Hardness of the samples was measured using a nano-indentation tester. Micro-scratch tests were performed under progressive and constant normal loads of 0-50 N. Dry wear behavior of the samples was studied using a ball-on-disk tribometer. The wear tests were carried out under various normal loads of 7.5, 15 and 30 N for sliding distances of 50, 100, 200 and 300 m using alumina balls as the counterface. The wear and scratch tracks were examined by scanning electron microscope and surface profilometer. The ODL samples showed higher hardness and lower plastic deformation as compared with Ti–6Al–4V. The brittle behavior of the ODL samples caused the formation of cracks and the development of large acoustic signals during scratching under normal loads of 40 and 50 N. The results also showed a higher scratch and wear resistance of the ODL samples compared with Ti–6Al–4V. However, the oxygen diffusion layer formed after 3 h of oxidation showed a sharp increase in the wear rate of the alloy under a normal load of 30 N and a sliding distance of 100 m.

Keywords: Ti–6Al–4V; Oxygen Diffusion Layer; Wear; Scratch; Normal load; Sliding distance.

1. Introduction

Ti-6Al-4V alloy is increasingly used in a wide variety of applications [1–3] and forms over 50% of the usage of titanium alloys in different industries [4]. However, a low wear resistance of Ti-6Al-4V could be a drawback for using in a dynamic contact [5]. The poor wear resistance of Ti-6Al-4V alloy is due to three interacting factors: (i) a low shear resistance [6], (ii) a higher slip systems compared with other hcp alloys [7] that results in a higher plastic deformation [5] and, therefore, formation of a larger real contact area during sliding [8], and (iii) formation of tribo-layer with a low durability on Ti-6Al-4V wear surface during dry sliding [9,10].

The wear resistance of Ti-6Al-4V has been improved by different surface engineering methods such as anodic oxidation (i.e., anodizing [10] and plasma electrolytic oxidation [11]), physical and chemical vapor deposition [12,13], surface melting and alloying [14], stirred friction processing [15], diffusion based treatment [16], thermal oxidation [17] and boost diffusion oxidation [18]. Among them, the thermal oxidation is an effective and environmentally friendly technique. Oxygen element has high affinity for titanium and, therefore, a very thin and adherent layer of titanium oxide (rutile) always covers the surface in the atmosphere [19]. Thermal oxidation results in an increase in the kinetics of the reaction and intentionally forms an oxide layer with various thicknesses on the surface; depending on the temperature and duration of the processing. The formation of a sound oxide layer, although, could improve the wear resistance of Ti-6Al-4V [20]; it needs a precise selection of oxidation parameters [21]. On the other hand, the oxide on the surface has a low capacity of load bearing due to its high fragility [22]. The boost diffusion oxidation (BDO) technique, which is developed by Dong et al. [18], contained two steps: (1) thermal oxidation at high temperature and (2) decomposition of the oxide within high vacuum at

high temperature. This technique could result in a deeply hardened layer [20]. However, it is costly and time consuming.

Oxygen atoms are also dissolved in titanium up to 34 at% [23] and enhance the mechanical properties (i.e., hardness and strength) of Ti-6Al-4V alloy [19]. During thermal oxidation, oxygen dissolution occurs in the titanium substrate due to inward diffusion of oxygen, which results in the formation of an Oxygen Diffusion Layer (ODL) beneath the oxide layer [24]. Thermal oxidation of titanium at a temperature higher than 800 °C and for a long period of time leads to thickening of the oxide layer [25]. The thick oxide layer could detach from the surface during cooling, which is due to: (i) a great mismatch between titanium and rutile lattices [26], (ii) a large ratio (1.7) of the oxide to titanium specific volumes [27] and (iii) a significant difference in the coefficients of thermal expansion between titanium and rutile [28]. Dearnley et al. [29] have investigated the oxidation behavior of CP-titanium at high temperatures. They found that the oxide layer with a thickness of about 20 µm formed at 800 °C for 36 hours had no durability, which was due to the presence of a large number of cracks on it. The layer finally peeled off from the oxide-ODL interface and removed from the surface.

In this study, a defective oxide layer and an underlying ODL were formed on Ti-6Al-4V alloy by atmospheric thermal oxidation at a temperature of 850 °C for three and six hours. Air quenching was used to remove the loose oxide from the surface and, subsequently, the properties of the ODLs were investigated. Nano-hardness measurements, scratch and dry wear resistance of the ODLs were studied and compared with Ti-6Al-4V alloy.

2. Experimental Procedure

A Ti–6Al–4V bar with a diameter of 32 mm was sliced to prepare disk samples, 4 mm in thickness. The chemical composition of Ti–6Al–4V was obtained using Optical Emission Spectroscopy (OES) and is listed in Table 1. The disks were polished with SiC grit papers, up to No. 600 to reach a surface roughness (R_a) of about 0.5 μm . The samples were then immersed in acetone and ultrasonically cleaned for 5 minutes. The prepared samples were heated in an atmospheric furnace with a heating speed of 5 $^{\circ}\text{C}\cdot\text{min}^{-1}$. Thermal oxidation was performed on the samples at a temperature of 850 $^{\circ}\text{C}$ for three and six hours. Subsequently, the samples were quenched in air and the oxide layer was mostly detached from the surface. Finally, the ODL samples treated for 3 h (3h-ODL) and 6 h (6h-ODL) were lightly polished to remove the remaining scales from the surfaces [30].

Table 1. Chemical composition of Ti–6Al–4V alloy (wt%)

Ti	Al	V	Fe	Mo	Si	Cu	W	Nb	Ni	Sn	Mn
Base	6.37	4.33	0.03	0.01	0.01	0.01	<0.01	0.008	<0.005	<0.005	<0.004

Nano-indentation tests were performed on the untreated and treated samples under a normal load of 10 mN with a loading/unloading rate of 0.2 $\text{mN}\cdot\text{s}^{-1}$. The variation of the applied load versus penetration depth were measured and plotted. Micro-scratch tests were carried out on the samples using a scratch tester (Millennium 200) under two different loading conditions: (i) under progressive normal load of 0-50 N with a constant loading rate of 100 $\text{N}\cdot\text{min}^{-1}$, and (ii) under constant normal loads of 10, 20, 40 and 50 N. A Rockwell diamond stylus with a radius of 200 μm was used to scratch the samples for a length of 5 mm at a speed of 10 $\text{mm}\cdot\text{min}^{-1}$. The variation of acoustic emission signals was also recorded during the tests. The critical loads, which resulted

in a failure during the tests, were detected by the variation of acoustic emission signals (i.e., peak formation) during the tests.

A ball-on-disk tribometer was used to evaluate the dry wear resistance of the alloy under normal loads of 7.5, 15 and 30 N at room temperature. The alumina balls with a hardness of 1550 Hv_{0.5} were used as the counterpart. The wear tests were carried out for various sliding distances of 50, 100, 200 and 300 m at a sliding speed of 0.1 m.s⁻¹. Before the tests, the samples were ultrasonically cleaned in an acetone bath. A balance with an accuracy of 10⁻⁴ g was used for measuring the mass of samples prior and after the tests to obtain the mass loss.

A HommelWerk surface profilometer was used to measure the depth of the wear and scratch tracks under the various normal loads. The surfaces of the tracks were further studied using Scanning Electron Microscope (SEM) and Energy Dispersive Spectroscopy (EDS). The nano-indentation, surface profilometry, scratch and wear experiments were repeated three times and the mean values and standard deviation were reported.

3. Results and discussion

3.1. Nano-indentation

Nano-indentation load as a function of the penetration depth were obtained for Ti-6Al-4V and the ODL samples and are plotted in Fig. 1. The penetration depth consisted of two different regions; (1) elastic depth where the deformation was recovered as the applied normal load was relieved; and (2) plastic depth that resulted in a permanent and unrecoverable indentation due to an applied normal load as shown typically for the indentation of Ti-6Al-4V by the dashed arrows in Fig. 1. Figure 1 shows a lower plastic penetration depth occurred in the ODL samples under a constant

normal load of 10 ± 0.1 mN. This resulted in higher nano-hardness [31] values of about 1020 Hv (10.0 GPa) and 1950 Hv (19.1 GPa) for 3h-ODL and 6h-ODL, respectively, compared with a hardness of 500 Hv (5.0 GPa) for Ti-6Al-4V. The work of plastic deformation (W_P), which roughly indicates the toughness of the samples and defines as the area under the curves was calculated and is also presented in Fig. 1. The work of plastic deformation of Ti-6Al-4V was about 78% and 174 % higher than the values for 3h-ODL and 6h-ODL, respectively. This revealed that as the hardness increased in the ODL samples, the amount of plastic deformation (i.e., plastic work) was limited resulting in a decrease in the toughness and, therefore, an increase in the brittleness.

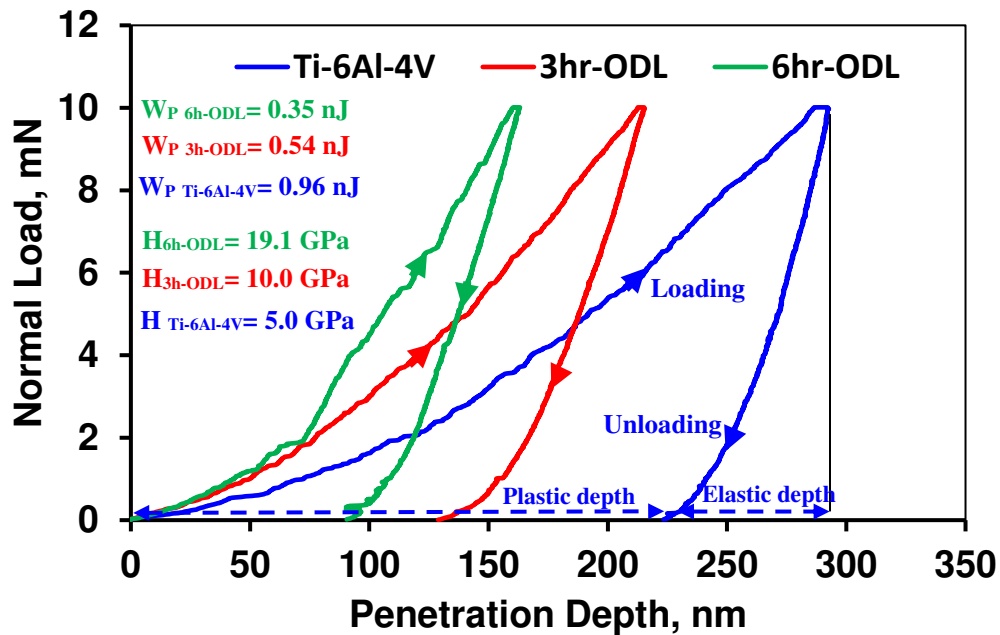


Fig. 1. Normal load versus penetration depth for Ti-6Al-4V, 3h-ODL and 6h-ODL samples. The values of the plastic deformation work (W_P) and hardness (H) of the samples are presented in the figure. The elastic and plastic depth are only shown for Ti-6Al-4V.

The lower work of plastic deformation of the ODLs could be attributed to the structural ordering and an increase in the c/a ratio of hcp structure of α -Ti, which resulted from the presence of oxygen atoms in the interstitial sites. Holmberg [32] has demonstrated that oxygen atoms are placed in every other layer of octahedral positions in the hcp structure of α -Ti and form an ordered structural arrangement. The structural ordering in titanium decreases its ability to plastic deformation and the toughness [33]. The axial ratio of c/a is 1.587 for hcp structure of titanium [34]. The oxygen atoms in the interstitial sites lead to an expansion in the hcp structure of α -Ti, during which “c” axis expands more than “a” axis. The expansion of the hcp structure increases with the increase in the oxygen content [35]. This results in a higher c/a ratio of 1.637 at the solubility limit of 34 at% [36]. The higher c/a ratio of the hcp structure decreased the compactness of planes and, therefore, slip systems of α -Ti(O). This limited plastic deformation and, therefore, lowered the work of plastic deformation in Fig. 1, i.e., the toughness (a higher brittleness) of the ODLs.

According to our previous study [30], the thickness of the ODL layers was measured to be about 30 μm and 60 μm on 3h-ODL and 6h-ODL samples, respectively. The interstitial oxygen concentration at the interface of the diffusion and oxide layer was always equal to the solubility limit of oxygen in titanium, i.e., 34 at.% [37]. Due to the higher diffusion time, the concentration of oxygen at any depth in the ODLs was higher in 6h-ODL, resulting in a higher hardness [30]. In addition, during thermal oxidation, the thickness of the initial oxide layer on the surface was increased by time. The thicker oxide layer on 6h-ODL sample could induce more residual stress due to the mismatch of coefficient of thermal expansion of the oxide and the substrate [26,27]. The higher residual stress may increase the defects (i.e., micro cracks) formed in oxide during thermal oxidation [24] where the oxygen atoms diffused more easily into the titanium substrate. This could also increase the oxygen content of the ODL at any depth in 6h-ODL as compared with 3h-ODL, which limited the plastic deformation and led to a higher hardness.

3.2. Scratch resistance

The progressive micro-scratch tests were performed on Ti-6Al-4V, 3h-ODL and 6h-ODL samples under normal loads of 0-50 N. During the tests, acoustic signals were detected and are shown in Fig. 2. The variations in the acoustic signal could indicate a change in the material response, i.e., crack formation and material failure under a normal load during scratching [38,39]. Figure 2a shows that there was no significant variation in the amplitude of acoustic signal over the range of the applied normal loads in Ti-6Al-4V. This may suggest that no meaningful cracks were likely formed within the scratch track as the normal load was increased. Figure 3 shows SEM images of the scratch tracks of Ti-6Al-4V under various normal loads of 10, 20, 40 and 50 N. The surface profile, depth, width, and cross-sectional area (A) of the valley formed by a scratch are also presented in the images. Fine plastic grooves were the main feature of the scratch tracks of Ti-6Al-4V as a result of sliding against the very hard counterpart, i.e., diamond stylus. Ti-6Al-4V has a high capability for plastic flow [34] during sliding. α -Ti with hcp structure which constitutes the main part of Ti-6Al-4V (i.e., about 90% of Ti-6Al-4V microstructure [36]) has a c/a ratio of 1.587 [23]. This ratio is lower than the value of 1.633 for an ideal hcp structure [40]. The lower c/a ratio results in more slip systems in Ti-6Al-4V compared with other hcp alloys. Therefore, a higher plastic deformation could be easily accommodated in Ti-6Al-4V, which could hinder the crack formation during sliding. The high ability of Ti-6Al-4V for plastic deformation was also resulted in the formation of raised lips on the edges of the tracks as shown in the surface profiles of the valleys in Fig. 3.

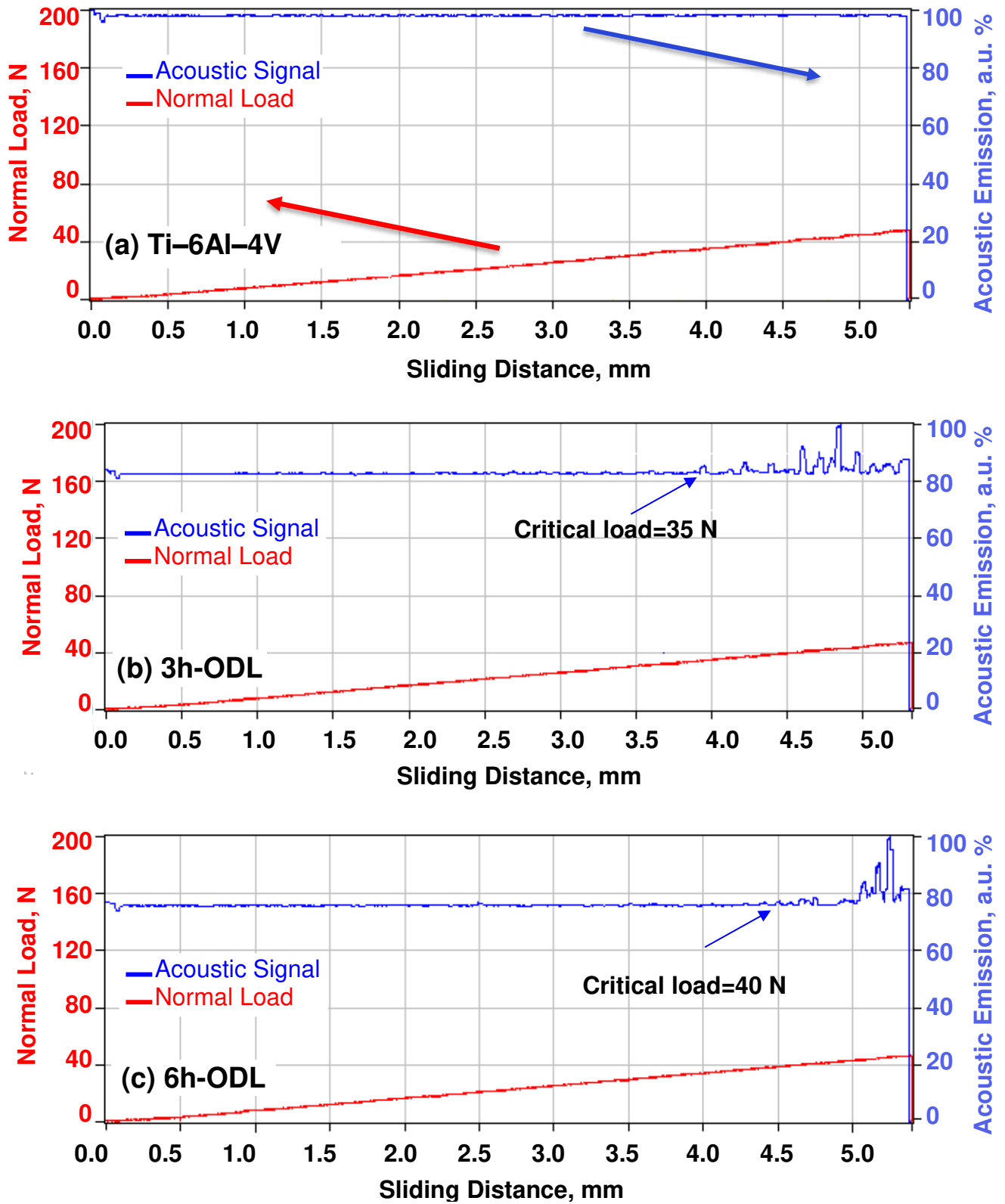


Fig. 2. Acoustic emission signal and normal load versus sliding distance during progressive scratch tests of (a) Ti-6Al-4V, (b) 3h-ODL and (c) 6h-ODL under a normal load range of 0-50 N at a sliding speed of 10 mm.min⁻¹ and a loading rate of 100 N.min⁻¹.

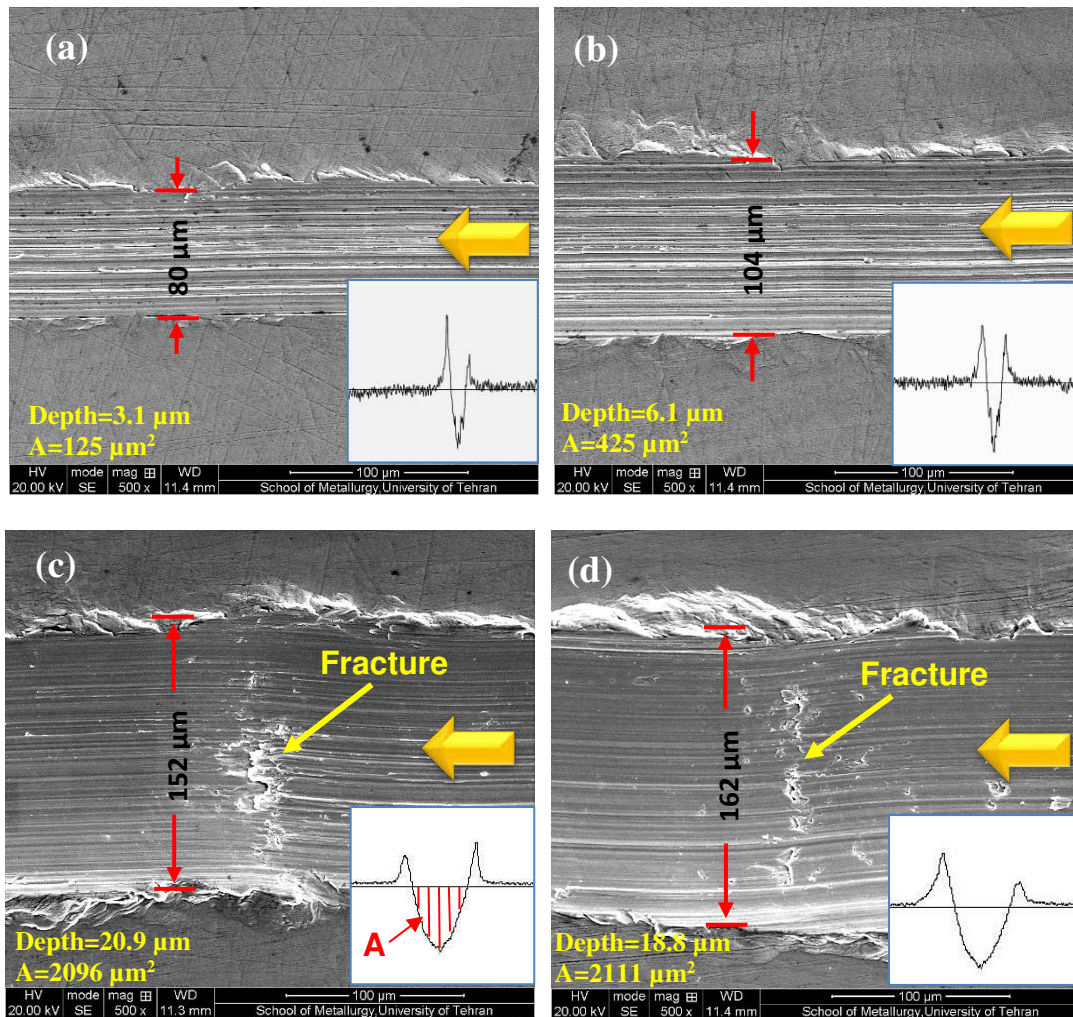


Fig. 3. SEM images of the scratch tracks of Ti–6Al–4V samples under a constant normal load of: (a) 10 N, (b) 20 N, (c) 40 N and (d) 50 N at a sliding speed of 10 mm.min⁻¹. The width of the tracks is specified in the images and the depth, cross sectional area (A) and profile of the valleys are presented on the lower side of the images. The thick arrows show the moving direction of the sample during the scratch test.

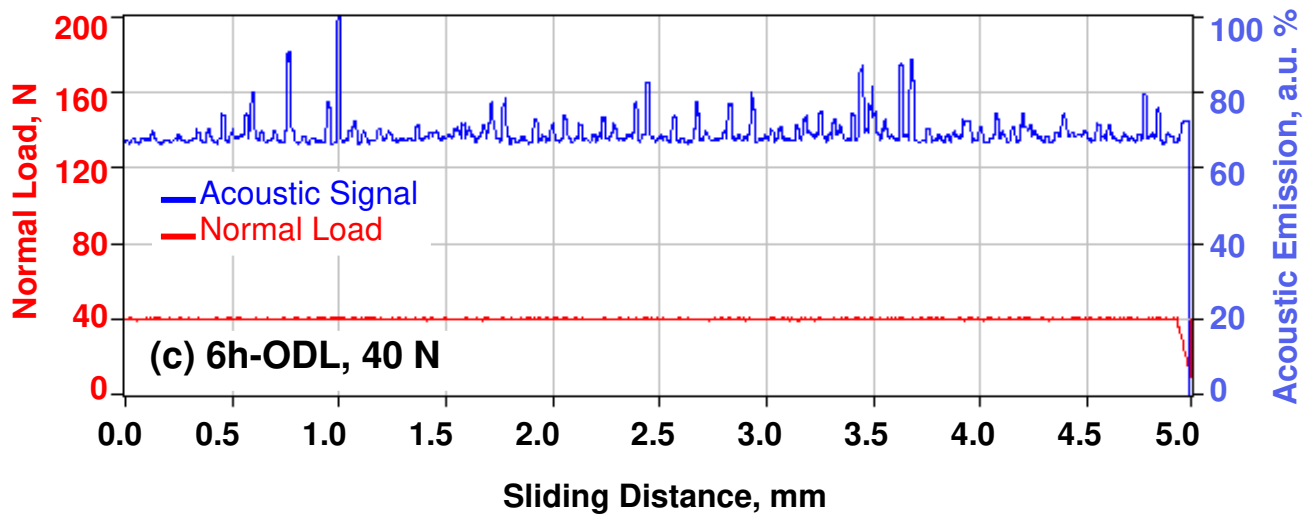
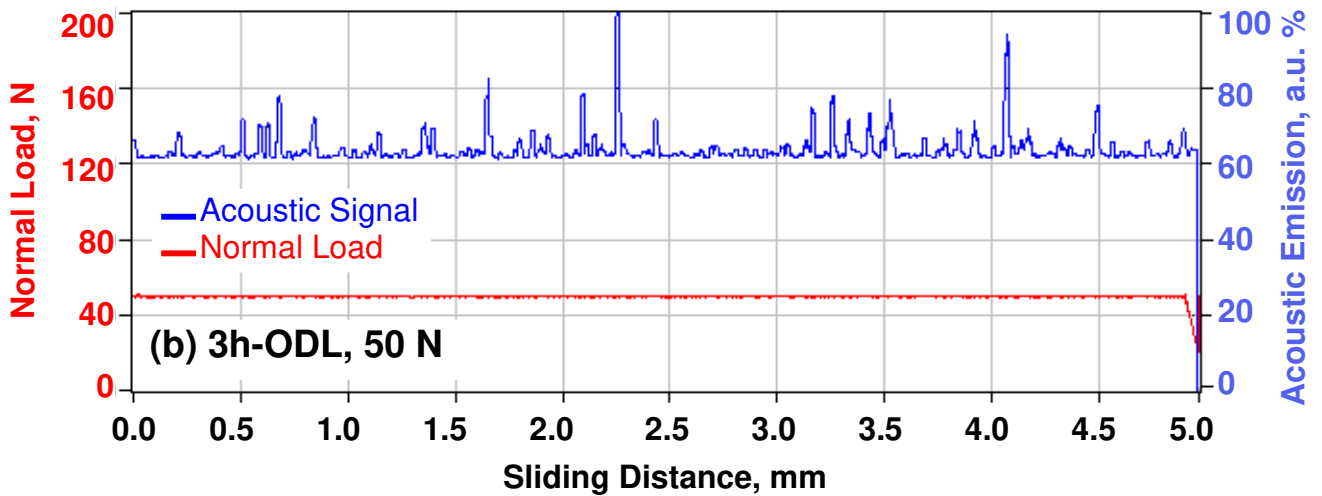
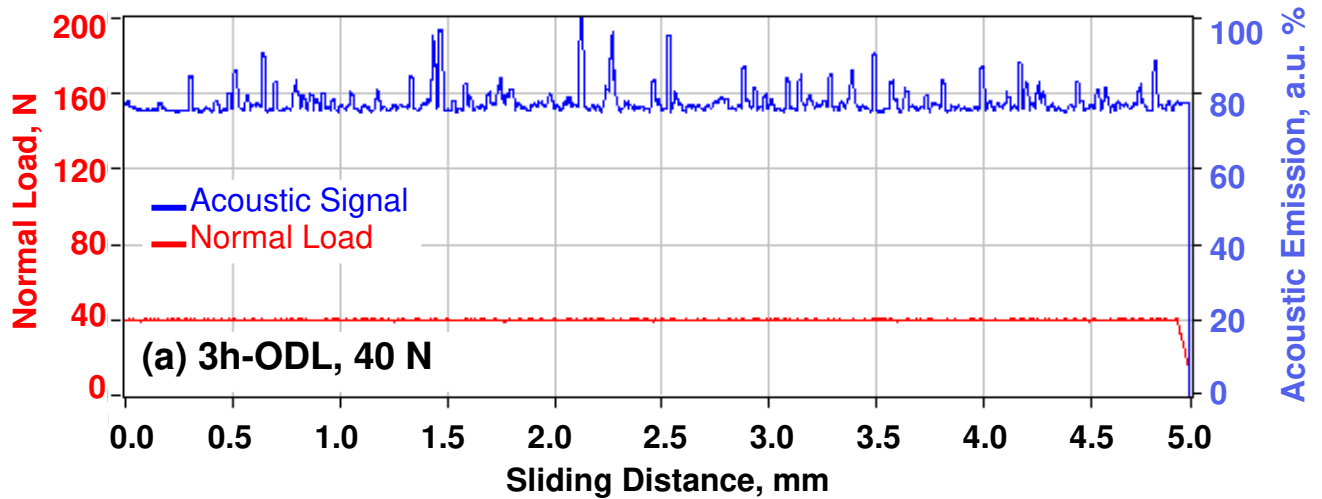
In scratch testing, a critical load is defined as the minimum normal load that results in material failure such as fracture and cracks during scratch test [35]. The first acoustic peak formed during the progressive scratch test could be considered to occur under a critical load. The acoustic emission signal of Fig. 2a does not show large peaks, however, the SEM images of Figs. 3c and d show some surface failures on the scratch tracks of Ti–6Al–4V under normal loads of 40 and 50 N. This was attributed to an excessive plastic flow, which was not accommodated by the alloy during

sliding. However, the failures were not detected by the acoustic signal in Fig. 2a, which was probably due to the higher ductile deformation, i.e., higher W_P , of Ti-6Al-4V during scratching.

Acoustic signals of the ODL samples during the progressive micro-scratching in Figs. 2b and c show a number of peaks under the normal loads higher than 35 N, which could indicate the formation of cracks on the scratch tracks. Comparing the acoustic signals in Fig. 2b and c shows that critical loads of about 35-40 N was achieved in ODLs. The acoustic peaks that occurred under these loads were due to the lower work of deformation and higher hardness of 3h-ODL and 6h-ODL diffusion layers compared with Ti-6Al-4V.

The scratch tests were also performed under constant normal loads of 40 and 50 N on 3h-ODL and 6h-ODL samples and the change in acoustic signals are shown in Fig. 4. The acoustic signals with large number of peaks during sliding confirmed the change in the material behavior under the higher normal loads in Figs. 2b and c. SEM images of the scratch tracks of the ODL samples under the normal loads of 20, 40 and 50 N are shown in Fig. 5. The depth, width, cross sectional area (A) and surface profile over the width of tracks are also presented in the images. The figure reveals that no cracks were formed on the ODL surfaces as a result of scratching under a normal load of 20 N. This confirms the acoustic emission signals in Figs. 2b and c, in which no peaks were observed under the lower normal loads (i.e., less than 35 N). Figure 5 also shows that there were some fractured regions (i.e., spallation [41]) on the edges of the scratch tracks with much smaller raised lips (shown in the surface profile in Fig. 5) compared with Ti-6Al-4V in Fig. 3. The friction between the diamond stylus and the ODL caused the maximum radial stress to occur at the sides of scratch track [42], resulting in cracks in the more brittle materials (i.e., ODLs). Therefore, at each side of the scratch tracks in Figs. 5 c-d, the cracks could mainly develop due to

the higher frictional forces at higher loads of 40 and 50 N and the lack of sufficient toughness leading to cohesive spallation [43].



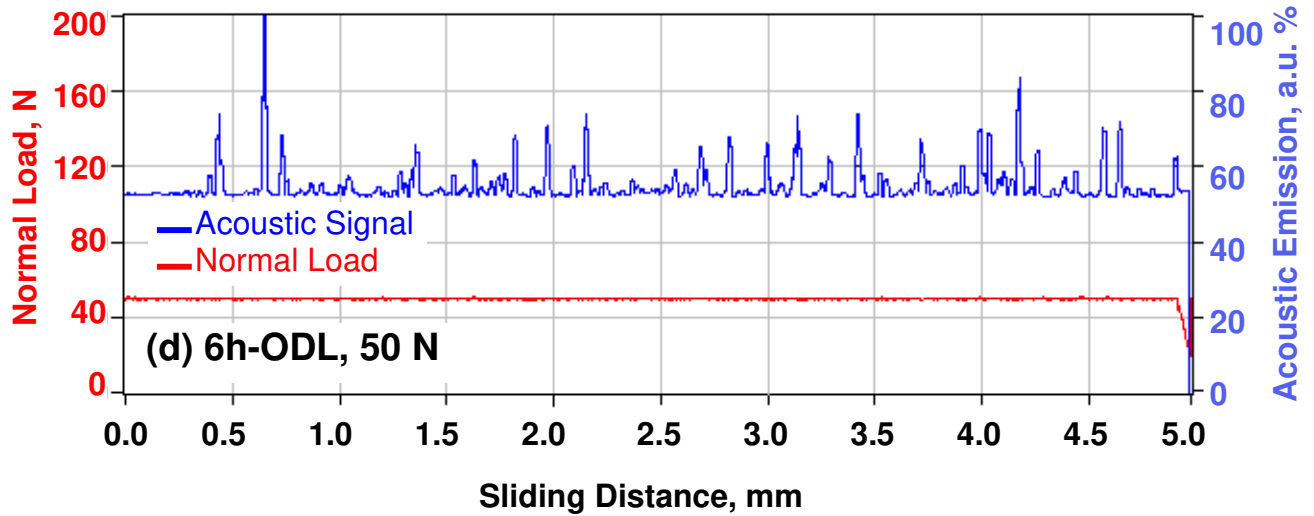


Fig. 4. Acoustic emission signal and normal load versus sliding distance during scratch test of; (a, b) 3h-ODL and (c, d) 6h-ODL under constant normal loads of 40 and 50 N at a sliding speed of $10 \text{ mm}\cdot\text{min}^{-1}$.

Figures 5d-f show that some semi-circular cracks were formed perpendicular to the sliding direction on the scratch tracks of 3h-ODL and 6h-ODL samples. Sliding under a normal load results in high tensile stresses at the rear of the moving contact region [8]. The high tensile stress generated under a high normal load on the surface of the ODL samples with a higher brittleness (i.e., lower work of plastic deformation) (Fig. 1) induced cracks perpendicular to the sliding direction as shown in Fig. 5. The higher toughness of 3h-ODL sample indicated in Fig. 1 hindered the formation of well-defined cracks under a normal load of 40 N in Fig. 5c and resulted in shorter cracks under a normal load of 50 N in Fig. 5e as compared with 6h-ODL sample in Figs. 5d and f. The spallation of the material on the edges and the lateral cracks within the scratch tracks were both responsible for the observed acoustic peaks for the ODL samples in Figs. 2 and 4.

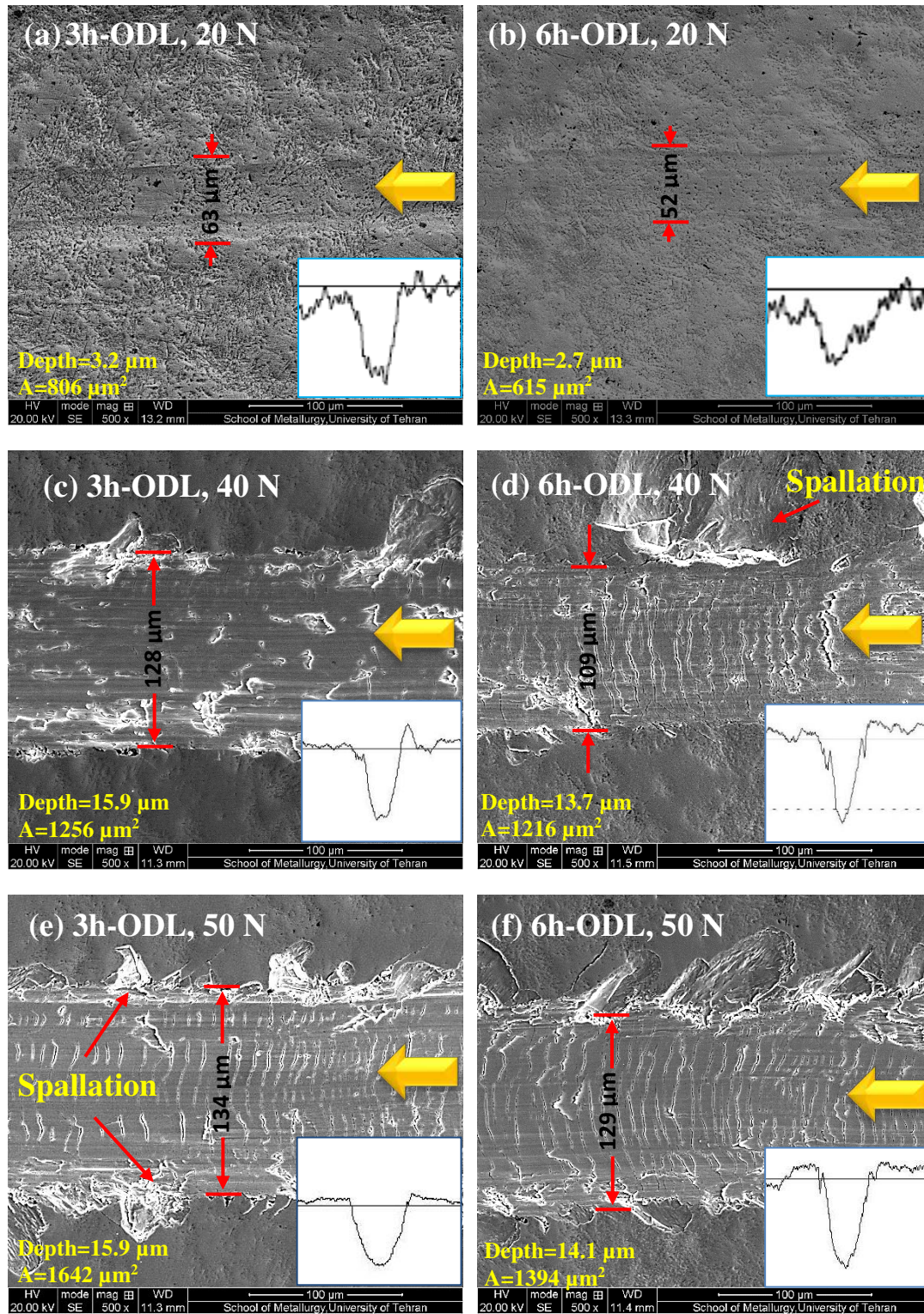


Fig. 5. Scratch tracks of: (a) 3h-ODL under a constant normal load of 20 N, (b) 6h-ODL under a constant normal load of 20 N, (c) 3h-ODL under a constant normal load of 40 N, (d) 6h-ODL under a constant normal load of 40 N, (e) 3h-ODL under a constant normal load of 50 N, and (f) 6h-ODL under a constant normal load of 50 N at a scratching speed of $10 \text{ mm} \cdot \text{min}^{-1}$. The width of the tracks is specified in the images and the depth, cross sectional area (A) and profile of the tracks are presented on the lower side of the images. The thick arrows show the moving direction of the sample during the scratch test.

Figure 5 also shows that the maximum depths of the scratch tracks were less than 16 μm for the ODL samples. The oxygen diffusion layer with the thickness of about 30 and 60 μm on 3h-ODL and 6h-ODL samples, respectively, indicated that the diamond stylus slid within the oxygen diffusion layers during the scratch tests. Comparing Figs. 3 and 5 revealed that the depth, width and cross sectional area of the tracks was lower in the ODL samples as compared with Ti-6Al-4V. Under a normal load of 50 N, for example, the ODLs produced by thermal oxidation for 3 and 6 h led to a decrease of about 22% and 34% in the cross sectional area of the scratch tracks. This implied a lower volume loss of the ODL samples than Ti-6Al-4V during the scratch tests. According to ASTM G 171 [44], a scratch hardness number could be calculated by dividing the applied normal load (P) by the projected area of the scratching contact (i.e., the hemispherical-tipped stylus) which is responsible for forming the scratch. The projected area of the contact surface is a semi-circle whose diameter is equal to the width of scratch track (w). The scratch number is presented in the following equation:

$$HS_P = \frac{8P}{\pi w^2} \quad \text{Equation (1)}$$

Where HS_P is the scratch hardness number (MPa), P is the applied normal load (N) and w is the scratch width (mm) as shown in Figs. 3 and 5. The scratch hardness number under a normal load of 50 N (i.e., HS_{50}) was typically calculated to be 4.85, 7.09 and 7.66 GPa for Ti-6Al-4V, 3h-ODL and 6h-ODL samples, respectively. Therefore, it could be concluded that although the more brittle behavior of the ODL samples in Fig. 1 resulted in the formation of cracks on the scratch surfaces in Fig. 5, their higher hardness and adequate toughness led to a higher scratch resistance as compared with Ti-6Al-4V under the applied loads.

3.3. Wear behavior

The variations of the wear rates and specific wear rates of the samples as a function of applied normal load for a sliding distance of 300 m are shown in Fig. 6. The wear rates of the ODL samples in Fig. 6a were lower than the untreated alloy, i.e., Ti-6Al-4V under various normal loads. Titanium atom with four valence electrons [23] is chemically active and prefers to bond with the counterparts during sliding in order to become more thermodynamically stable. This results in the high adhesion between titanium and its counterpart during sliding [18]. The higher wear rate of Ti-6Al-4V could be due to its lower hardness (Fig. 1) as well as its low shear strength [45] and high adhesion between the mating surfaces [18]. The coefficients of friction of the samples were measured during sliding and the results under a normal load of 7.5 N are typically presented in Fig. 7. A lower average coefficient of friction with larger fluctuations was obtained for Ti-6Al-4V compared with 3h-ODL and 6h-ODL samples. The higher instability in the coefficient of friction of Ti-6Al-4V could be related to the higher adhesion between the mating surfaces in Ti-6Al-4V /alumina contact than the ODL/alumina contact. On the other hand, the low shear strength of Ti-6Al-4V alloy [45] could be the reason of its lower average coefficient of friction as compared with the ODLs.

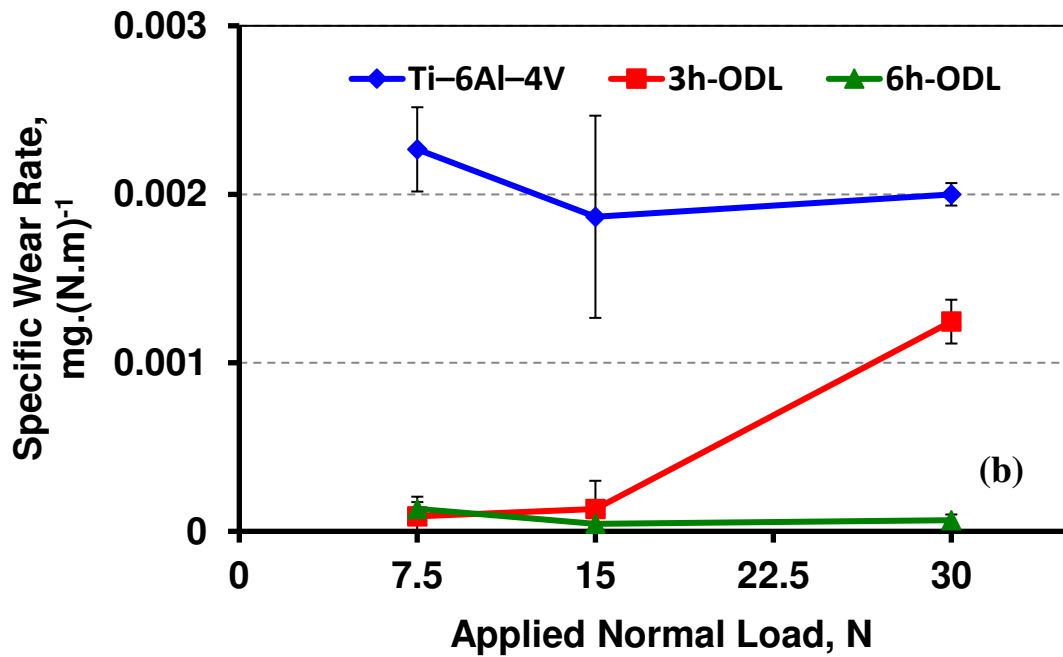
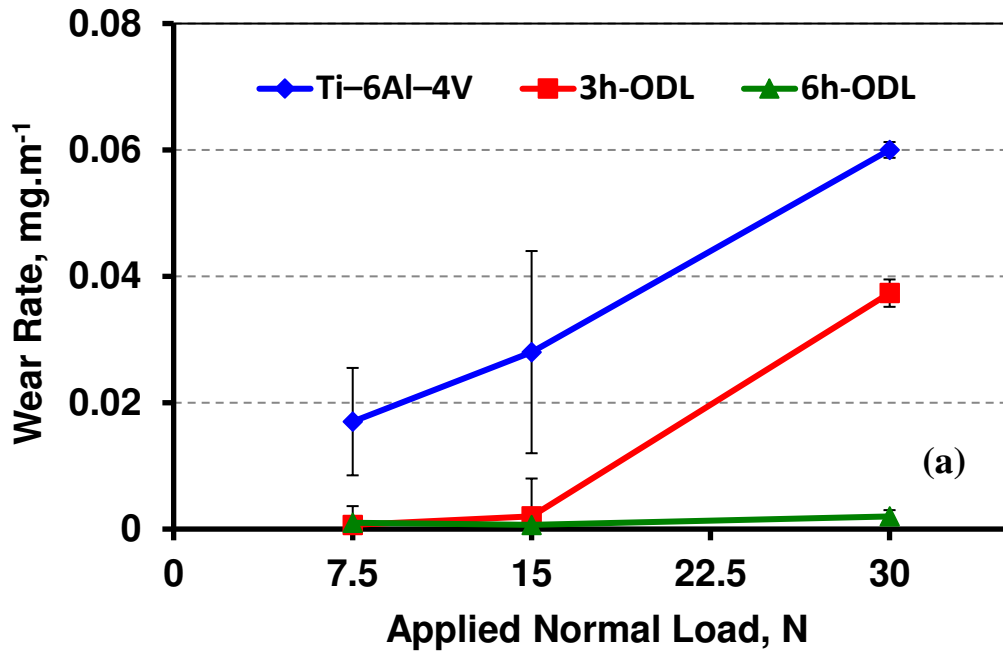


Fig. 6. Variations of: (a) wear rate and (b) specific wear rates of Ti-6Al-4V, 3h-ODL and 6h-ODL samples with applied normal load at a sliding distance of 300 m.

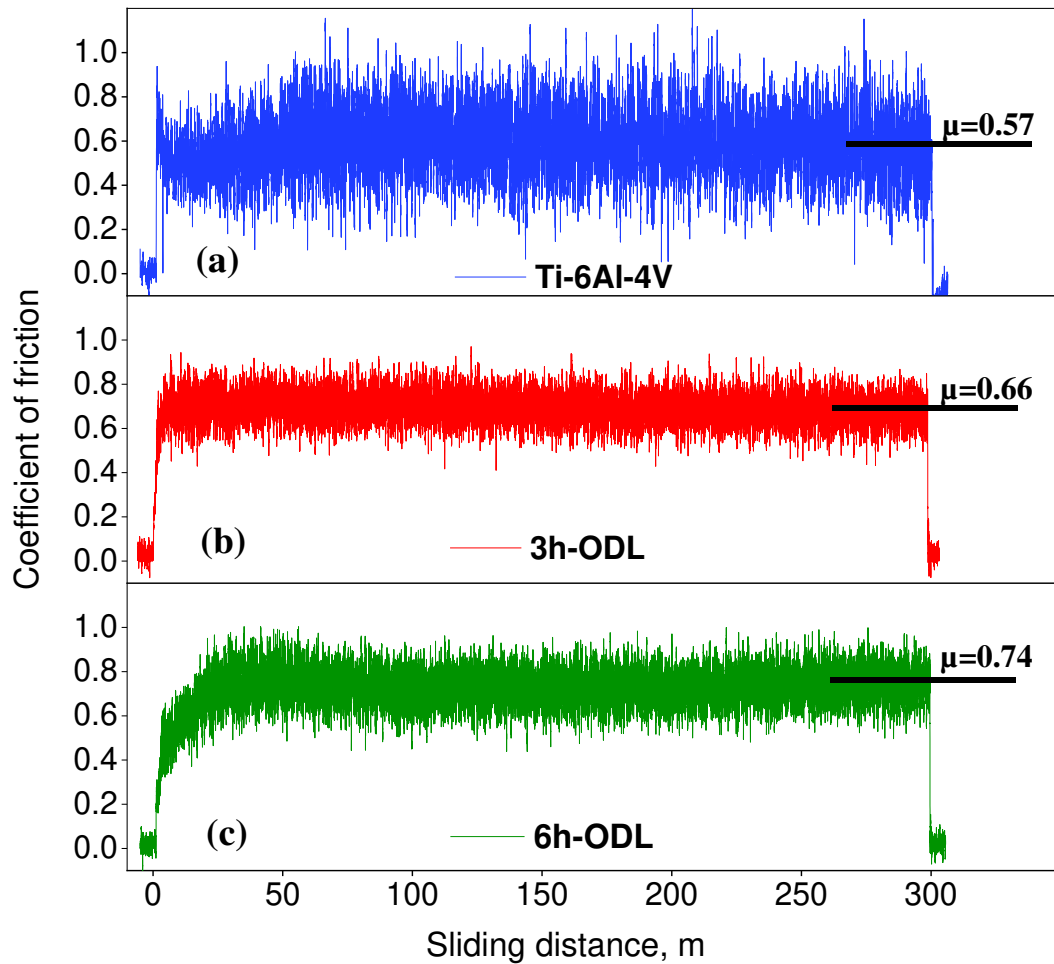


Fig. 7. Variations of coefficient of friction as a function of sliding distance against alumina ball under a normal load of 7.5 N; (a) Ti-6Al-4V, (b) 3h-ODL and (c) 6h-ODL.

The wear results in Fig. 6 were further in agreement with the results of the higher scratch resistance of the ODL samples compared with Ti-6Al-4V that was discussed in the previous section. Figure 6b shows a drop in the specific wear rate of Ti-6Al-4V as the normal load increased from 7.5 to 15 N followed by an almost constant value at the higher normal load of 30 N. This could suggest a milder wear of Ti-6Al-4V under normal loads of 15 and 30 N compared with 7.5 N. Figure 8 shows the SEM micrographs of the wear tracks of Ti-6Al-4V under various normal

loads. Some grooves could be observed on the wear surfaces of Ti-6Al-4V under all normal loads that indicated plastic deformation and ploughing. This could be due to the low hardness and high work of plastic deformation (W_p) of Ti-6Al-4V (Fig. 1) that provided high ability for plastic deformation. The EDS analysis of the bright and dark regions on the wear tracks are presented in Table 2. The dark regions contained a higher oxygen content (14-18 wt%) compared with the bright regions (3-6 wt%) indicating the formation of an oxygen-rich tribo-layer on the wear tracks [4]. The oxygen content of the oxide patches (i.e., dark region) under various normal loads could indicate the formation of a comparable tribo-layer thickness on the wear track. Some cracks perpendicular to the sliding direction were observed on the brittle oxide tribo-layers in Figs. 8b, d and f under various normal loads. This could be due to the induced high tensile stresses behind the moving contact during sliding [8].

The SEM images in Fig. 8 also show no significant change on the morphology of wear surfaces of Ti-6Al-4V under various normal loads. However, Fig. 6b shows a decrease in the specific wear rate of Ti-6Al-4V as the normal load was increased from 7.5 N to 15 and 30 N. This could be attributed to the higher work hardening of the alloy during sliding [4] under the higher normal loads that increased the hardness and the strength of the substrate. This led to a better support of the oxygen-rich tribo-layer by the substrate and a lower specific wear rate under the higher loads. Figure 8 shows a more compact tribo-layer formed under normal loads of 15 and 30 N, which protected the wear surfaces compared with a normal load of 7.5 N. Moreover, Figs. 8a and b reveal a higher generation of wear debris detached from the oxide patches, which resulted in a higher specific wear rate (Fig. 6b).

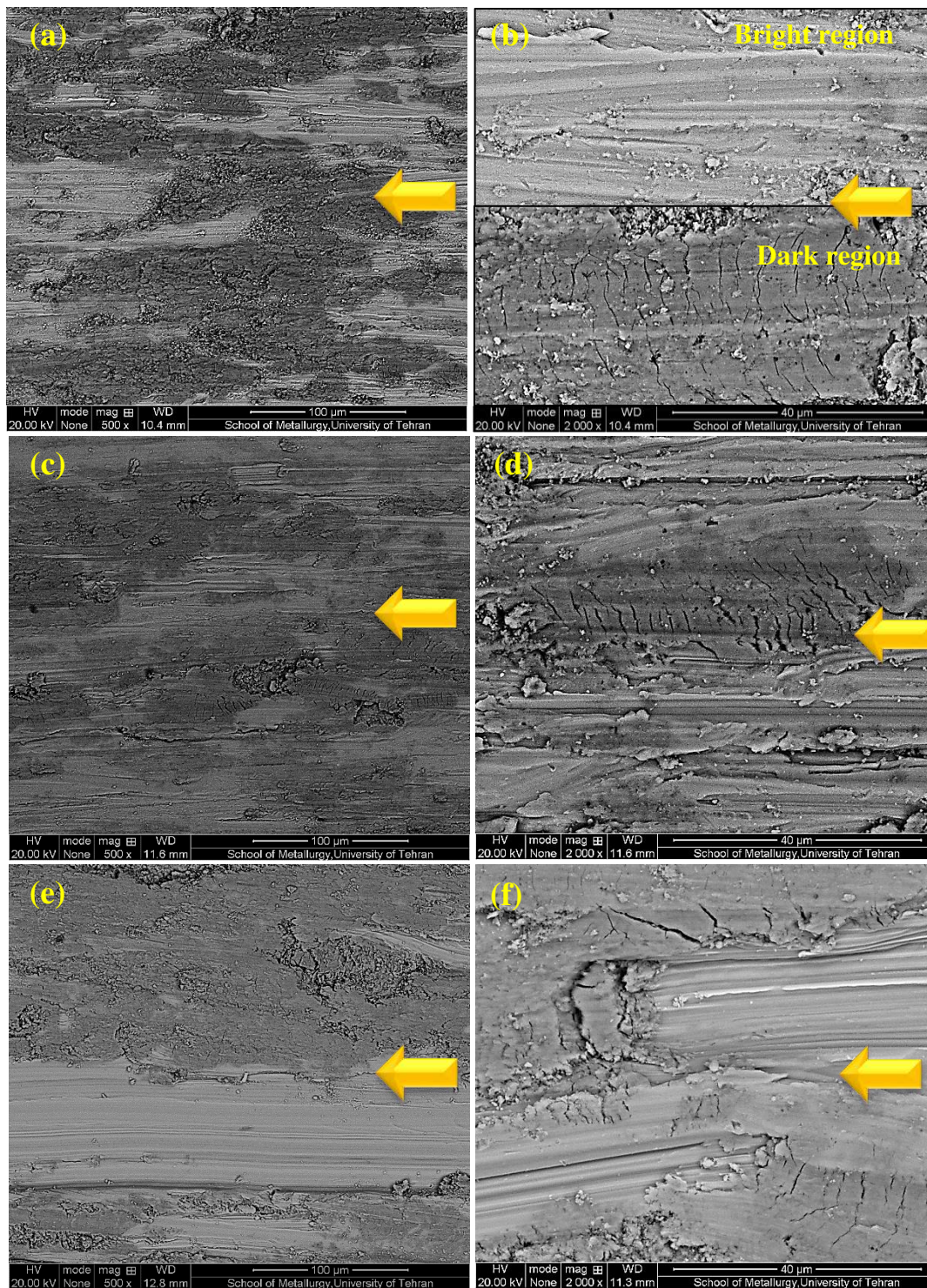


Fig. 8. SEM backscatter images of the wear surfaces of Ti-6Al-4V at a sliding distance of 300 m under normal loads of: (a, b) 7.5 N, (c, d) 15 N and (e, f) 30 N. The arrows show the sliding direction.

Table 2. The EDS analysis (wt%) of the bright and dark regions on the wear tracks of Ti-6Al-4V under various normal loads in Fig. 8

Normal load, N	Region	Ti	Al	V	O
7.5	Bright	90.9	6.5	1.4	1.3
	Dark	71.3	8.7	1.8	18.2
15	Bright	87.0	6.0	1.1	5.9
	Dark	75.1	5.8	2.0	17.1
30	Bright	91.8	5.4	---	2.8
	Dark	79.8	6.3	---	14.0

Figure 6a shows that a twice increase in the normal load from 15 to 30 N resulted in 18 times increase in the wear rate of 3h-ODL and a sharp increase in the specific wear rate in Fig. 6b. In this condition, the wear rate of 3h-ODL was only 38% lower than Ti-6Al-4V, suggesting a more severe wear occurred under a normal load of 30 N as compared with the lower normal loads of 7.5 and 15 N. Figure 6 indicate that unlike 3h-ODL sample, no sharp increase occurred in the wear rate and specific wear rate of 6h-ODL sample under various normal loads.

Figures 9 and 10 show SEM micrographs of the wear surfaces of 3h-ODL and 6h-ODL samples, respectively, at a sliding distance of 300 m under various normal loads. The EDS analysis of the bright and dark regions of Figs. 9 and 10 are listed in Table 3. The table shows a higher amount of oxygen on the dark patches of the ODL wear surfaces (except on 3h-ODL under 30 N) compared with the analysis of the dark regions on Ti-6Al-4V under the same conditions in Table 2. The oxygen content of the oxygen-rich patches on the ODL wear surfaces was from both the patches and the ODL subsurface. Furthermore, the formation of a thicker or a more compact oxygen-rich tribo-layer on the wear surface of ODLs could also result in a higher oxygen content compared with the tribo-layers on Ti-6Al-4V.

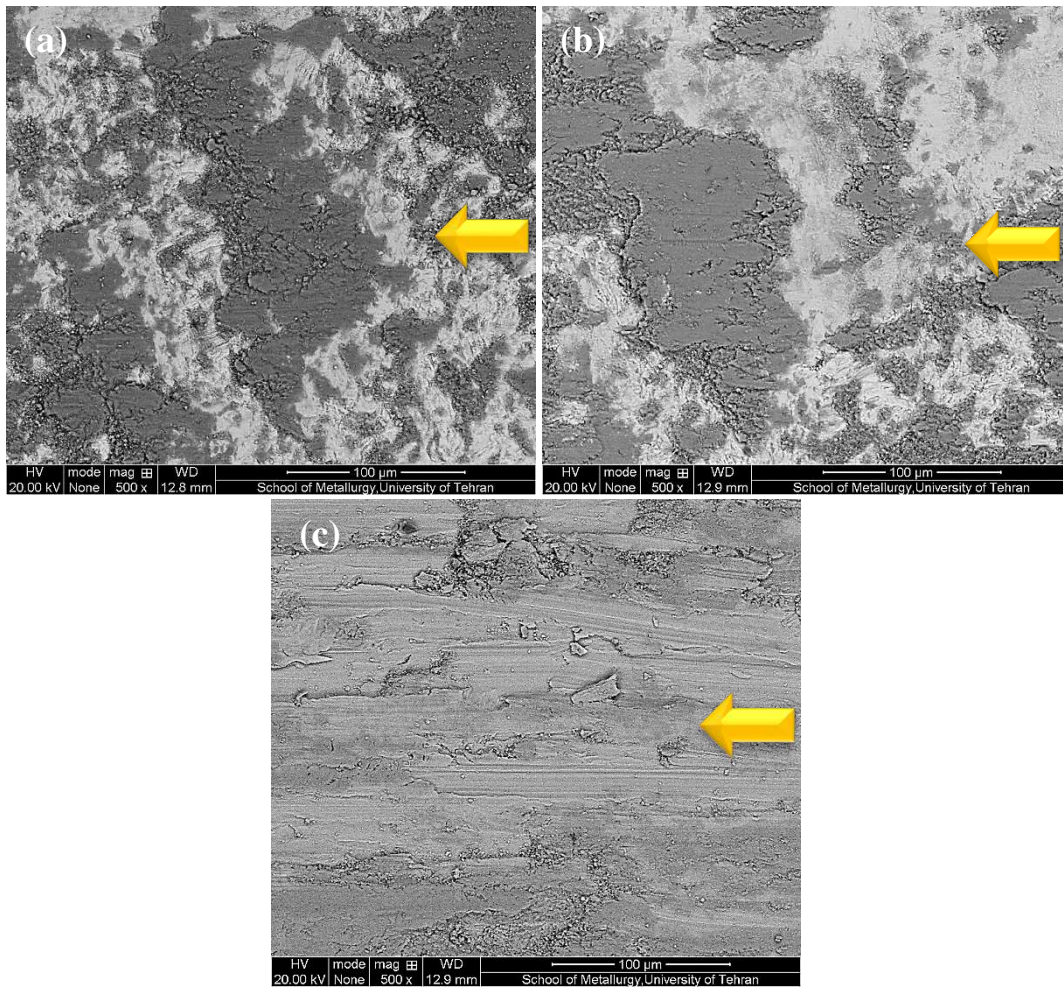


Fig. 9. SEM backscatter images of the wear surfaces of 3h-ODL at a sliding distance of 300 m under normal loads of: (a) 7.5 N, (b) 15 N and (c) 30 N. The arrows show the sliding direction.

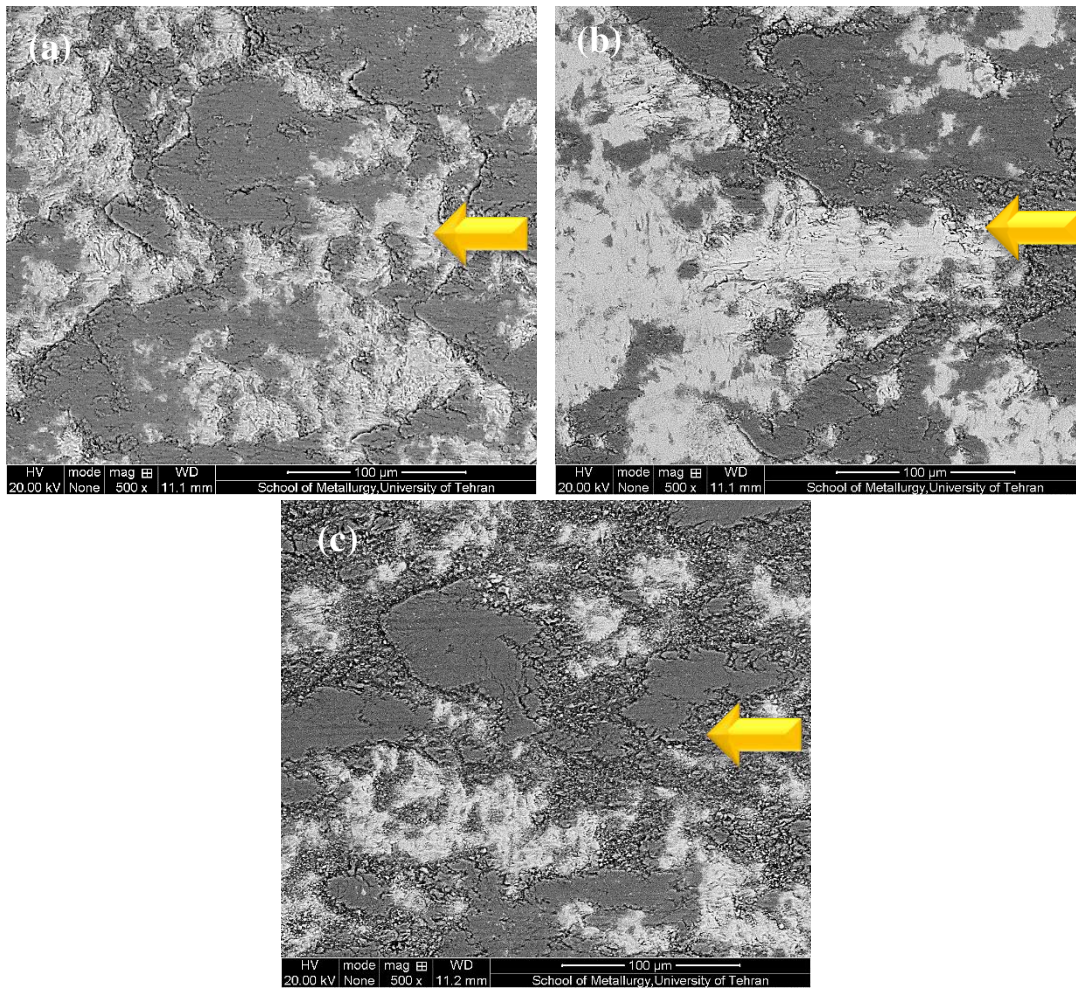


Fig. 10. SEM backscatter images of the wear surfaces of 6h-ODL at a sliding distance of 300 m under normal loads of: (a) 7.5 N, (b) 15 N and (c, d) 30 N. The arrows show the sliding direction.

The more compact oxygen-rich tribo-layers formed on the ODL with a higher strength and hardness (i.e., Fig. 1) was also responsible for a decrease of about 95% in the wear rate of 3h-ODL under normal loads of 7.5 and 15 N, and 6h-ODL under all normal loads compared with Ti-6Al-4V in Fig. 6a after 300 m of sliding. In addition, the similar features and the amount of coverage of the patches in Figs. 9a, b and 10 could suggest the occurrence of a same oxidative wear mechanism. This resulted in a little change in the specific wear rates of 3h-ODL under normal loads of 7.5 and 15 N and 6h-ODL under all normal loads in Fig. 6b.

Table 3. EDS analysis (wt%) of the bright and dark regions on the wear tracks of 3h-ODL and 6h-ODL under various normal loads in Figs. 9 and 10

Sample	Normal load, N	Region	Ti	Al	V	O
3h-ODL	7.5	Bright	68.3	4.7	1.5	25.5
		Dark	42.9	10.3	1.7	44.3
	15	Bright	83.4	5.24	1.1	10.3
		Dark	48.6	7.7	1.2	42.7
	30	Bright	92.4	6.6	1.0	0.0
		Dark	74.5	6.1	1.4	18.0
6h-ODL	7.5	Bright	79.8	5.5	1.4	13.3
		Dark	45.7	11.1	1.0	42.2
	15	Bright	82.6	5.2	1.3	10.9
		Dark	48.4	9.7	1.3	40.6
	30	Bright	71.0	4.9	1.2	22.9
		Dark	48.1	6.7	0.9	44.3

Table 3 indicates that the oxygen content of the tribo-layers on the wear surface of 3h-ODL sample under a normal load of 30 N was as low as that for Ti–6Al–4V in Table 2, which might suggest the removal of the ODL during sliding. The average depth of the wear tracks of the samples under various normal loads is illustrated in Fig. 11. A continuous increase in the wear depth with normal load was observed and was consistent with the trend of the wear rates in Fig. 6a. Under normal loads of 7.5 and 15 N, the wear depths (i.e., lower than 10 μm) were less than the thickness of ODL on 3h-ODL sample, i.e., 30 μm [30]. Figure 11 also shows that the depth of wear tracks of 6h-ODL sample under various normal loads were about 6 μm , which was much lower than the depth of the oxygen diffusion layer, i.e., 60 μm [30]. Therefore, it could be stated that the process of sliding occurred on the oxygen diffusion layer under the testing conditions after 300 m of sliding. For 3h-ODL sample under a normal load of 30 N, however, a sharp increase in the wear depth to a value of 80 μm was observed in Fig. 11, which was much deeper than thickness of the ODL (30 μm). This suggests that the oxygen diffusion layer was completely worn out and the

substrate material (Ti-6Al-4V) was exposed to wear. The EDS analysis in Table 3 shows no oxygen for the brighter regions on the wear surface of 3h-ODL sample under a normal load of 30 N, which also confirmed the removal of the ODL at this condition.

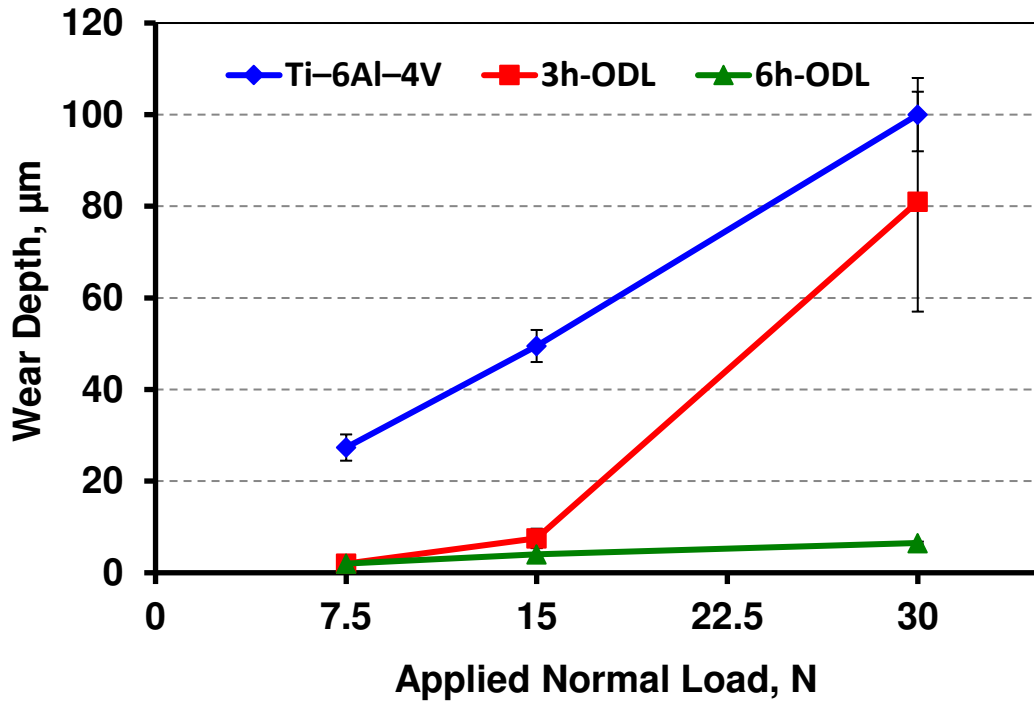


Fig. 11. Variations of the wear depth of Ti-6Al-4V, 3h-ODL and 6h-ODL samples with normal load at a sliding distance of 300 m.

The variation of the wear rate and wear depth of Ti-6Al-4V and ODLs under a normal load of 30 N with sliding distance is presented in Fig. 12. Comparing Figs. 12a and b suggests that 3h-ODL layer with a thickness of 30 µm was worn out after 100 m of sliding. The change in the mechanical properties of the wear surfaces from a high strength and hardness 3h-ODL to a low wear-resistant Ti-6Al-4V occurred between sliding distance of 50 and 100 m, which was also responsible for the sharp increase in the wear and specific wear rates of 3h-ODL as shown in Fig. 6. Figure 12a also shows a similar trend in the wear behavior of 3h-ODL and Ti-6Al-4V which could further indicate the similarities of the contacts for sliding distances higher than 50 m. Similar features of

plastic deformation such as grooves on the wear surface of 3h-ODL and Ti-6Al-4V under a normal load of 30 N after 300 m of sliding in Figs. 9c and 8 further indicated the removal of the ODL in 3h-ODL.

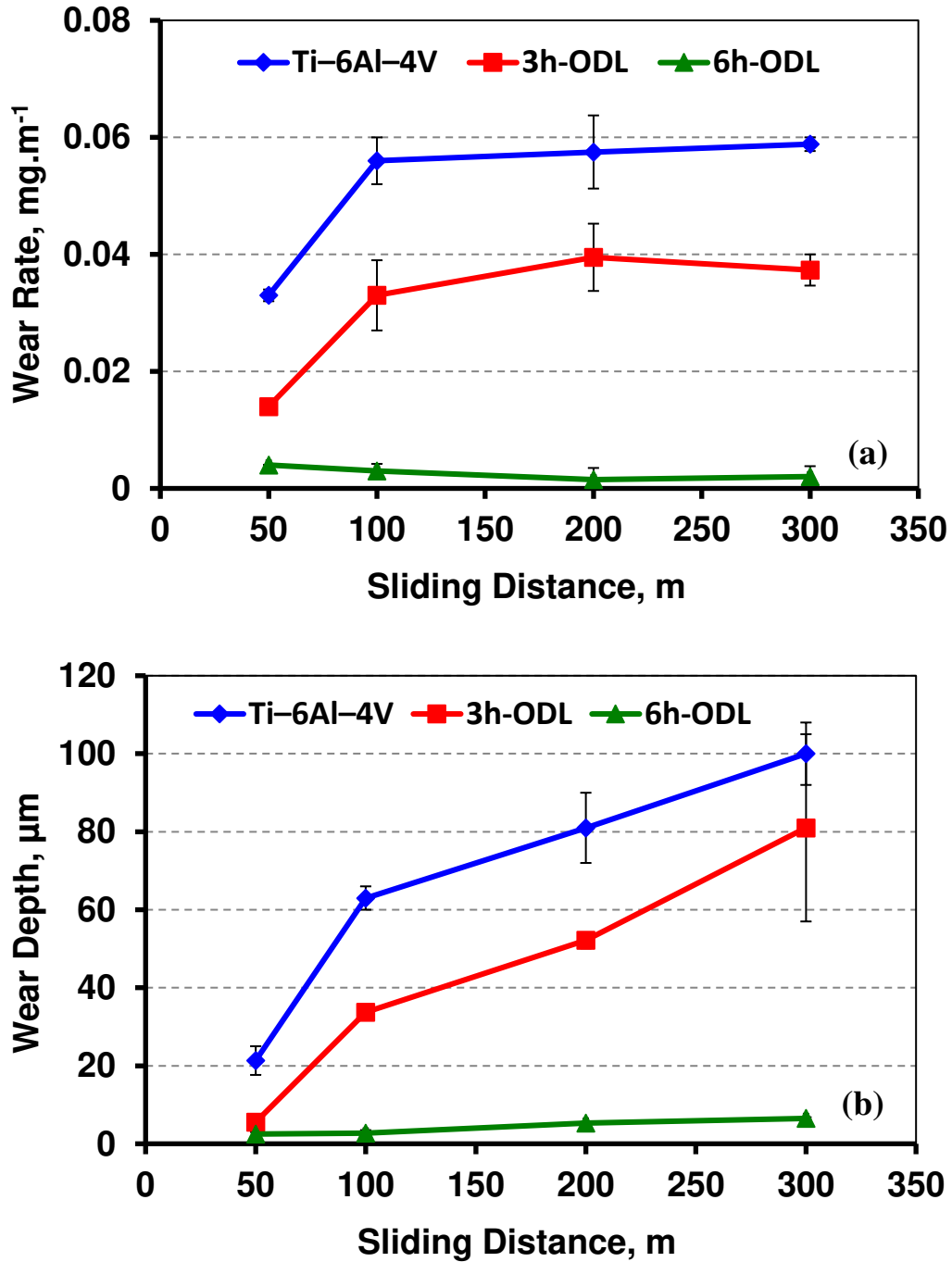


Fig. 14. Variations of: (a) wear rates and (b) wear depth of Ti-6Al-4V, 3h-ODL and 6h-ODL samples with sliding distance under a normal load of 30 N.

Figure 12 shows that the oxygen diffusion layer with a thickness of 60 μm in 6h-ODL was not removed during sliding under a normal load of 30 N at various sliding distances, which could indicate the significant effect of the formation of ODL in reducing wear and maintaining a constant specific wear rate during sliding the wear mechanism with sliding distance.

4. Conclusions

1. Oxygen diffusion layer on Ti-6Al-4V produced by thermal oxidation showed higher hardness of 19.1 GPa for 6h-ODL and 10.0 GPa for 3h-ODL as compared with 5.0 GPa for untreated Ti-6Al-4V. The results also indicated a lower toughness in the ODL samples due to the diffusion of oxygen.
2. The scratch tests in the ODLs revealed a limited plastic deformation, a more brittle behavior and formation of cracks under the normal loads higher than 35-40 N. However, the scratch resistance of the ODL samples was higher than Ti-6Al-4V.
3. The wear results showed a decrease of about 95% in the wear rate of the ODL samples under normal loads of 7.5 and 15 N as compared with Ti-6Al-4V. The amounts of decrease in the wear rate under a normal load of 30 N were about 38% and 5% for 3h-ODL and 6h-ODL samples compared with Ti-6Al-4V, respectively.
4. The oxygen diffusion layer on 3h-ODL sample was totally worn out under a normal load of 30 N after a sliding distance of 50 to 100 m, which resulted in sharp increase in the wear rate. The removal of ODL during sliding under a normal load of 30 N caused 18 times higher wear rate in 3h-ODL sample compared with 6h-ODL after a sliding distance of 300 m.

References

- [1] C. Leyens, M. Peters, *Titanium and Titanium Alloys*, 2003. doi:10.1002/3527602119.
- [2] M. Niinomi, Recent research and development in titanium alloys for biomedical applications and healthcare goods, *Sci. Technol. Adv. Mater.* 4 (2003) 445–454. doi:10.1016/j.stam.2003.09.002.
- [3] S. Seong, O. Younossi, W. Goldsmith, *Titanium Industrial Base, Price Trends, and Technology Initiatives*, First, Rand, 2009.
- [4] Y.S. Mao, L. Wang, K.M. Chen, S.Q. Wang, X.H. Cui, Tribo-layer and its role in dry sliding wear of Ti-6Al-4V alloy, *Wear.* 297 (2013) 1032–1039. doi:10.1016/j.wear.2012.11.063.
- [5] K.G. Budinski, Tribological properties of titanium-alloys, *Wear.* 151 (1991) 203–217. doi:10.1016/0043-1648(91)90249-T.
- [6] S. V. Kailas, S.K. Biswas, Sliding wear of titanium, *J. Tribol.* 119 (1997) 31. doi:10.1115/1.2832476.
- [7] A.A. Salem, S.R. Kalidindi, R.D. Doherty, S.L. Semiatin, Strain hardening due to deformation twinning in alpha-titanium: Mechanisms, *Metall. Mater. Trans. A.* 37 (2006) 259–268. doi:10.1007/s11661-006-0171-2.
- [8] I. Hutchings, *Tribology: friction and wear of engineering materials*, 1st Ed., Butterworth-Heinemann, London, 1992.
- [9] G. Straffelini, A. Molinari, Dry sliding wear of Ti-6Al-4V alloy as influenced by the counterface and sliding conditions, *Wear.* 236 (1999) 328–338. doi:10.1016/S0043-1648(99)00292-6.
- [10] A. Molinari, G. Straffelini, B. Tesi, T. Bacci, Dry sliding wear mechanisms of the Ti6Al4V alloy, *Wear.* 208 (1997) 105–112. doi:10.1016/S0043-1648(96)07454-6.
- [11] S. Aliasghari, P. Skeleton, G.E. Thompson, Plasma electrolytic oxidation of titanium in a phosphate/silicate electrolyte and tribological performance of the coatings, *Appl. Surf. Sci.* 316 (2014) 463–476. doi:10.1016/j.apsusc.2014.08.037.
- [12] M. Rizzi, G. Gatti, M. Migliario, L. Marchese, V. Rocchetti, F. Renò, Effect of zirconium nitride physical vapor deposition coating on preosteoblast cell adhesion and proliferation onto titanium screws, *J. Prosthet. Dent.* 112 (2014) 1103–1110. doi:10.1016/j.prosdent.2014.04.010.
- [13] J.C. Nable, S. Nosheen, S.L. Suib, F.S. Galasso, Atmospheric pressure chemical vapor deposition of titanium nitride on metals, *Surf. Coatings Technol.* 200 (2006) 2821–2826. doi:10.1016/j.surfcoat.2005.02.171.
- [14] R. Yazdi, S.F. Kashani-Bozorg, Microstructure and wear of in-situ Ti/(TiN + TiB) hybrid composite layers produced using liquid phase process, *Mater. Chem. Phys.* 152 (2015). doi:10.1016/j.matchemphys.2014.12.026.

- [15] L.H. Wu, D. Wang, B.L. Xiao, Z.Y. Ma, Tool wear and its effect on microstructure and properties of friction stir processed Ti-6Al-4V, *Mater. Chem. Phys.* 146 (2014) 512–522. doi:10.1016/j.matchemphys.2014.04.002.
- [16] P. Stratton, M. Graf, Wear of diffusion hardened Ti-6Al-4V sliding against tool steel, *Wear.* 268 (2010) 612–616. doi:10.1016/j.wear.2009.10.009.
- [17] S. Wang, Z. Liao, Y. Liu, W. Liu, Influence of thermal oxidation duration on the microstructure and fretting wear behavior of Ti6Al4V alloy, *Mater. Chem. Phys.* 159 (2015) 139–151. doi:10.1016/j.matchemphys.2015.03.063.
- [18] H. Dong, T. Bell, Enhanced wear resistance of titanium surfaces by a new thermal oxidation treatment, *Wear.* 238 (2000) 131–137. doi:10.1016/S0043-1648(99)00359-2.
- [19] F.H. Froes, ed., *Titanium: Physical Metallurgy Processing and Application*, 1st Editio, ASM International, Ohio, 2015.
- [20] F. Borgioli, E. Galvanetto, F. Iozzelli, G. Pradelli, Improvement of wear resistance of Ti-6Al-4V alloy by means of thermal oxidation, *Mater. Lett.* 59 (2005) 2159–2162. doi:10.1016/j.matlet.2005.02.054.
- [21] M. Jamesh, S. Kumar, T.S.N. Sankara Narayanan, Effect of thermal oxidation on corrosion resistance of commercially pure titanium in acid medium, *J. Mater. Eng. Perform.* 21 (2011) 902–907. doi:10.1007/s11665-011-9970-8.
- [22] R. Bailey, Y. Sun, Corrosion and tribocorrosion performance of thermally oxidized commercially pure titanium in a 0.9% NaCl solution, *J. Mater. Eng. Perform.* 24 (2015) 1669–1678. doi:10.1007/s11665-015-1441-1.
- [23] H. Margolin, P. Farrar, The physical metallurgy of titanium alloys, *Ocean Eng.* 1 (1969) 329–345. doi:10.1016/0029-8018(69)90035-3.
- [24] H. Guleryuz, H. Cimenoglu, Oxidation of Ti-6Al-4V alloy, *J. Alloys Compd.* 472 (2009) 241–246. doi:10.1016/j.jallcom.2008.04.024.
- [25] S. Kumar, T.S.N.S. Narayanan, S.G.S. Raman, S.K. Seshadri, Thermal oxidation of CP-Ti: Evaluation of characteristics and corrosion resistance as a function of treatment time, *Mater. Sci. Eng. C.* 29 (2009) 1942–1949. doi:10.1016/j.msec.2009.03.007.
- [26] G.P. Burns, Titanium dioxide dielectric films formed by rapid thermal oxidation, *J. Appl. Phys.* 65 (1989) 2095–2097. doi:10.1063/1.342856.
- [27] C. Boettcher, Deep case hardening of titanium alloys with oxygen, *Surf. Eng.* 16 (2000) 148–152. doi:10.1179/026708400101517053.
- [28] H. Dong, A. Bloyce, P.H. Morton, T. Bell, Surface engineering to improve tribological performance of Ti-6Al-4V, *Surf. Eng.* 13 (1997) 402–406. doi:10.1179/sur.1997.13.5.402.
- [29] P.A. Dearnley, K.L. Dahm, H. Çimenoglu, The corrosion-wear behaviour of thermally oxidised CP-Ti and Ti-6Al-4V, *Wear.* 256 (2004) 469–479. doi:10.1016/S0043-1648(03)00557-X.

- [30] R. Yazdi, H.M. Ghasemi, C. Wang, A. Neville, Bio-corrosion behaviour of oxygen diffusion layer on Ti-6Al-4V during tribocorrosion, *Corros. Sci.* (2017). doi:10.1016/j.corsci.2017.08.031.
- [31] A.C. Fischer-Cripps, *Nanoindentation*, Third edit, Springer Science & Business Media, London, 2011. doi:10.1007/978-1-4419-9872-9.
- [32] B. Holmberg, Disorder and order in solid solutions of oxygen in α -titanium, *Acta Chem. Scand.* 16 (1962) 1245. doi:10.3891/acta.chem.scand.16-1245.
- [33] Z. Liu, G. Welsch, The effects of oxygen and heat treatment on microstructures and mechanical properties of alpha and beta titanium alloys, *Metall. Trans. A.* 19A (1988) 527–542. <http://link.springer.com/article/10.1007/BF02649267>.
- [34] F.H. Froes, ed., *Principles of Alloying Titanium*, in: *Titan. Phys. Metall. Process. Appl.*, First Edit, ASM International, Ohio, 2015: pp. 51–74.
- [35] P. Hedenqvist, M. Olsson, S. Jacobson, S. Söderberg, Failure mode analysis of TiN-coated high speed steel: In situ scratch adhesion testing in the scanning electron microscope, *Surf. Coatings Technol.* 41 (1990) 31–49. doi:10.1016/0257-8972(90)90128-Y.
- [36] S. Weissmann, A. Sherier, Strain distribution in oxidized alpha titanium crystals, in: R.I. Jaffee, N.E. Promisel (Eds.), *Sci. , Technol. Appl. Titan.*, Pergamon press, London, 1966: pp. 441–451.
- [37] S. Zabler, Interstitial oxygen diffusion hardening - a practical route for the surface protection of titanium, *Mater. Charact.* 62 (2011) 1205–1213. doi:10.1016/j.matchar.2011.10.012.
- [38] K. Farokhzadeh, A. Edrissy, G. Pigott, P. Lidster, Scratch resistance analysis of plasma-nitrided Ti – 6Al – 4V alloy, *Wear.* 302 (2013) 845–853. doi:10.1016/j.wear.2013.01.070.
- [39] J. Sekler, P.A. Steinmann, H.E. Hintermann, The scratch test - different critical load determination techniques, *Surf. Coat. Technol.* 36 (1988) 519–529. doi:10.1016/0257-8972(88)90179-x.
- [40] P.G. Partridge, The crystallography and deformation modes of hexagonal close-packed metals, *Rev. Lit. Arts Am.* 12 (1967) 169–194. doi:10.1179/mtlr.1967.12.1.169.
- [41] BS EN 1071-3, *Advanced technical ceramics - Methods of test for ceramic coatings*, (2005).
- [42] S. J. Bull, Failure modes in scratch adhesion testing, *Surf. Coatings Technol.* 50 (1991) 25–32.
- [43] P. Nledengvist, S. Hogmark, Experiences from scratch testing of tribological PVD coatings, *Tribol. Int.* 30 (1997) 507–516. doi:10.1016/S0301-679X(97)00014-5.
- [44] ASTM G171-03, *Standard test method for scratch hardness of materials using a diamond stylus*, ASTM Int. (2012) PA 19428-2959. United States.
- [45] Q.Y. Zhang, Y. Zhou, L. Wang, X.H. Cui, S.Q. Wang, Investigation on tribo-layers and

their function of a titanium alloy during dry sliding, *Tribol. Int.* 94 (2016) 541–549.
doi:10.1016/j.triboint.2015.10.018.